The Cryosphere
Discussions

Open Access

Impact of snow cover on CO$_2$ dynamics in Antarctic pack ice

N.-X. Geilfus[1,2,3]**, J.-L. Tison**[2]**, S. F. Ackley**[4]**, S. Rysgaard**[1,5,6]**, L. A. Miller**[7]**, and B. Delille**[3]

[1]Arctic Research Centre, Aarhus University, Aarhus, Denmark
[2]Laboratoire de Glaciologie, Université Libre de Bruxelles, Bruxelles, Belgium
[3]Unité d'Océanographie Chimique, Université de Liège, Liège, Belgium
[4]Department of Geological Sciences, University of Texas at San Antonio, San Antonio, TX, USA
[5]Centre for Earth Observation Science, University of Manitoba, Winnipeg, Canada
[6]Greenland Climate Research Centre, Greenland Institute of Natural Resources, Nuuk, Greenland
[7]Centre for Ocean Climate Chemistry, Institute of Ocean Sciences, Fisheries and Oceans, Canada, Sidney, BC, Canada

Correspondence to: N.-X. Geilfus (geilfus@biology.au.dk)

TCD

8, 3263–3295, 2014

Impact of snow cover on CO$_2$ dynamics in Antarctic pack ice

N.-X. Geilfus et al.

Title Page

Abstract	Introduction
Conclusions	References
Tables	Figures

|◀ | ▶|

◀ | ▶

Back | Close

Full Screen / Esc

Printer-friendly Version

Interactive Discussion

Full Screen / Esc

Printer-friendly Version

Interactive Discussion

Abstract

Temporal evolution of $p\mathrm{CO_2}$ profiles in sea ice in the Bellingshausen Sea, Antarctica, in October 2007 shows that the CO_2 system in the ice was primarily controlled by physical and thermodynamic processes. During the survey, a succession of warming and cold events strongly influenced the physical, chemical and thermodynamic properties of the ice cover. Two sampling sites with contrasting characteristics of ice and snow thickness were sampled: one had little snow accumulation (from 8 to 25 cm) and larger temperature and salinity variations than the second site, where the snow cover was up to 38 cm thick and therefore better insulated the underlying sea ice. We confirm that each cooling/warming event was associated with an increase/decrease in the brine salinity, total alkalinity (TA), total dissolved inorganic carbon ($T\mathrm{CO_2}$), and in situ brine and bulk ice CO_2 partial pressures ($p\mathrm{CO_2}$). Thicker snow covers muted these changes, suggesting that snow influences changes in the sea ice carbonate system through its impact on the temperature and salinity of the sea ice cover. During this survey, $p\mathrm{CO_2}$ was undersaturated with respect to the atmosphere both in situ, in the bulk ice (from 10 to 193 µatm), and in the brine (from 65 to 293 µatm), and the ice acted as a sink for atmospheric CO_2 (up to 2.9 mmol m^{-2} d^{-1}), despite the underlying supersaturated seawater (up to 462 µatm).

1 Introduction

Sea ice formation and melting may have a strong impact on the carbon cycle of polar oceans (e.g., Rysgaard et al., 2011; Delille et al., 2014). However, processes related to freezing and melting of sea ice, as well as their impact on CO_2 exchanges with the atmosphere, are still poorly understood (Parmentier et al., 2013). Detailed studies have been conducted on sea ice inorganic carbon chemistry and the impact of sea ice in the carbon cycle and the CO_2 exchanges between atmosphere, sea ice, and the ocean, only over the last decade (Semiletov et al., 2004; Zemmelink et al., 2006; Rysgaard

et al., 2007, 2011, 2012; Delille et al., 2007, 2014; Miller et al., 2011; Papakyriakou and Miller 2011; Geilfus et al., 2012a, 2013; Nomura et al., 2010a, 2013). These studies have shown that in both hemispheres, CO_2-carbonate chemistry in sea ice and brine is heterogeneous and variable, leading to complex CO_2 dynamics.

The CO_2 chemistry of sea ice seems to be highly dependent on brine salinity, which is controlled by ice temperature (Weeks, 2010). Both brine concentration during ice growth and brine dilution during ice melt play major roles in the carbonate system dynamics within sea ice (Papadimitriou et al., 2004; Nomura et al., 2010a; Geilfus et al., 2012a). In parallel, temperature affects pCO_2 due to the temperature dependence of both the dissociation constants of the carbonate system and the Henry's Law constant for CO_2. Brine concentration/dilution can be associated with precipitation/dissolution of calcium carbonate within the sea ice, also promoting an increase/decrease in the in situ brine pCO_2 (Papadimitriou et al., 2004, 2008; Rysgaard et al., 2007, 2012, 2013; Geilfus et al., 2012a, 2013). Biological processes, such as primary production and respiration, can also affect the CO_2-carbonate system within sea ice (Thomas and Dieckmann, 2010; Dieckmann and Hellmer, 2010; Delille et al., 2007). Finally, brine and gas transport within sea ice and across the air–ice and ice–water interfaces affect TA, TCO_2, and CO_2 distributions within the ice, together with the overall sea ice content of CO_2.

During the ice-covered period, snow gradually accumulates on the ice surface. Although snow thickness and distribution are variable and primarily result from the wind-induced redistribution of snow during storms (Weeks, 2010), the impact of snow cover on the thermal evolution of sea ice can be significant (Massom et al., 2001). Snow, which has a low thermal conductivity compared to sea ice (Massom et al., 2001), provides thermal insulation between the cold air and the ice. The presence of a thick snow cover also affects the isostatic balance, potentially resulting in negative freeboard, i.e. the snow–ice interface is submerged below the seawater level. If the sea ice is permeable throughout the entire ice column (with a high brine volume, which is controlled by temperature and salinity; Golden et al., 1998, 2007), the negative freeboard causes

Full Screen / Esc

Printer-friendly Version

Interactive Discussion

vertical flooding of the snow–ice interface through the open brine channels. Therefore, snow accumulation could strongly impact the CO$_2$-carbonate system within sea ice by regulating the ice temperature and the extent of flooding. The impact of snow on the CO$_2$ exchanges between sea ice and the atmosphere has previously been discussed by Nomura et al. (2010b); these authors suggested that a snow cover thicker than 9 cm could prevent any CO$_2$ exchanges between the ice and the atmosphere, and that melting snow can act as a physical barrier to CO$_2$ fluxes.

In this study, we examine the temporal evolution of the in situ brine and bulk ice pCO$_2$ profiles associated with physical and biogeochemical variables in the sea ice cover of two contrasting study sites, named "Brussels" and "Liège" that were sampled five times each between 1 and 23 October 2007, during the Sea Ice Mass Balance in Antarctic (SIMBA) cruise (Bellingshausen Sea, Antarctica) (Fig. 1) (Lewis et al., 2011). We describe how snow cover affects the temperature and salinity at both stations and outline the impact of these changes on the inorganic carbon dynamics within sea ice and brine and the related air–ice CO$_2$ fluxes. We also discuss the difference between the dynamics of the in situ bulk ice and brine pCO$_2$.

2 Study site, materials and methods

2.1 Selection of study site

The Sea Ice Mass Balance in the Antarctic (SIMBA) cruise investigated the physical and biological interactions between the ocean, sea ice, snow cover and atmosphere in the Bellingshausen Sea, onboard the RV *Nathaniel B. Palmer* (NBP) in October 2007. During this ~ one-month experiment, the vessel was moored to a first year sea–ice floe, the Ice Station Belgica (ISB), south of Peter I Island, at approximately 69–71° S and 90–95° W (Fig. 1). The station was chosen for its wide variety of ice types and snow cover (Lewis et al., 2011), characteristic of the greater region. Furthermore, the size of the ice floe (~ 5 km^2) had to be large enough to survive the duration of the field experiment.

Sampling was conducted at two distinct sites based on: (i) maximum homogeneity of the surface properties within each site, to reduce spatial variability; (ii) the contrast in ice and snow properties between the sites; and (iii) maximum distance from the ship (0.8 and 1.1 km), to prevent sample contamination. Each site was 100 m × 60 m and organized so as to avoid trace metal and organic matter contamination of the samples (Lewis et al., 2011). Each station was sampled at 5 day intervals: the Brussels site (low snow cover, at 0.8 km) was sampled on 1, 6, 11, 16, and 21 October (station names: Bxl 1 to 5), and the Liège site (high snow cover, at 1.1 km) was sampled on 3, 8, 13, 18, and 23 October (station names: Lg 1 to 5) (Fig. 2).

2.2 Sampling procedures

Ice cores were collected using an electro-polished stainless steel corer using an electric drill head, connected by a long cord to the power supply generator, which was located downwind from the sampling site. Cores were immediately wrapped in polyethylene bags and placed in an insulated box filled with gel packs pre-cooled to −30 °C, in order to limit the brine drainage from samples (Tison et al., 2008) and brought back to the ship laboratory. Sackholes (Gleitz et al., 1995) for collecting brines were drilled to four depths: 15, 30, 40, and 50 cm at the Brussels site; and 15, 30, 60 and 90 cm at the Liège site. Each sackhole was covered with a plastic lid to prevent contamination from falling snow. Brine seeped into the sackholes for 10 to 60 min before collection using a peristaltic pump (Cole Palmer, Masterflex-Environmental Sampler). Under-ice seawater was collected using the same peristaltic pump, with the inlet positioned at the ice–water interface, and at 1 and 30 m depths. On each sampling date, ice cores, brines and seawater were collected, and analyzed for a full range of physical and biogeochemical variables, including temperature (T), salinity (S), water stable isotopes of δ^{18}O, chlorophyll a (Chl a), total alkalinity (TA), pH$_T$, and in situ CO$_2$ partial pressure (pCO$_2$). Brine samples for pH$_T$ and TA analyses were only collected from the shallowest (at 0 to 15 cm depth) and at 0 to 40 cm depth at the Brussels site and 0 to 60 cm depth at the Liège site sackholes.

2.3   Materials and methods

The ice temperature was measured immediately after extraction of the ice core, using a calibrated temperature probe (TESTO 720, ±0.1 °C precision) inserted into pre-drilled holes ($\sim$ 5 cm intervals), perpendicular to the core sides. In the field, the ice core ded-
5   icated to bulk ice salinity measurements was cut into 5 cm thick slices and stored in separate, closed containers. Back in the ship laboratory, the ice was melted at room temperature, and bulk ice salinity on the practical salinity scale was determined from conductivity, using a portable calibrated Orion 3-Star conductivity meter with a precision of ±0.1. Brine volumes were calculated for each core using measured bulk ice salinities
10   and ice temperatures according to Cox and Weeks (1983) for ice temperatures below −2 °C and according to Leppäranta and Manninen (1988) for ice temperatures within the range −2 to 0 °C.

Aliquots (10 mL) of the bulk melted sea ice samples were transferred to gas tight vials to perform δ^{18}O measurements at the Australian Antarctic CRC. Isotope ratios
15   were measured with a dual-inlet VG SIRA mass spectrometer using the conventional water-CO$_2$ equilibration method. Accuracy with respect to VSMOW is ±0.12 ‰.

The pH of the sea–ice brines and seawater was measured using a Metrohm com-bined electrode calibrated on the total hydrogen ion scale (pH$_T$) using TRIS (2-amino-2-hydroxymethyl-1.3-propanediol) and AMP (2-aminopyridine) buffers prepared at salin-
20   ities of 35 and 75 according to the formulations proposed by DOE (1994). Measure-ments of pH$_T$ were carried out as soon as possible after the return to the ship laboratory (typically less than 2 h after sampling). Samples were maintained at low temperature, as close as possible to their in situ temperature (typically below 3 °C). The pH electrode was calibrated at temperatures ranging from 0 to 4 °C and at salinities ranging from 35
25   to 75. The accuracy of the pH$_T$ measurements was ±0.01 pH unit (Frankignoulle and Borges, 2001).

Total alkalinity in the brines and underlying seawater was measured by open-cell titration with HCl 0.1 M, and the endpoints were determined according to Gran (1952).

Routine analyses of Certified Reference Materials provided by A. G. Dickson, Scripps Institution of Oceanography, verified that TA accuracy was better than $\pm 4\,\mu mol\,kg^{-1}$. Total inorganic carbon (TCO_2) and pCO_2 (denoted as pCO_{2calc}) were calculated from TA and pH_T using the CO_2 acidity constants of Mehrbach et al. (1973) refit by Dickson and Millero (1987) and other constants advocated by DOE (1994). We assumed that the CO_2 dissociation constants were applicable at subzero temperatures, as suggested by Marion (2001) and Delille et al. (2007).

Brine and underlying seawater pCO_2 were measured in situ using a custom-made equilibration system (Geilfus et al., 2012a). The system consisted of a membrane contactor equilibrator (Membrana, Liqui-cell) connected to a non-dispersive infrared gas analyzer (IRGA, Li-Cor 6262) via a closed air loop. Brine and airflow rates from the equilibrator and IRGA, respectively, were approximately 2 and $3\,L\,min^{-1}$. Temperature was simultaneously measured in situ, within the sackholes or under-ice water, and at the equilibrator outlet using Li-Cor temperature sensors. Temperature correction of the pCO_2 values was applied assuming that the Copin Montégut (1988) relation is valid at low temperatures and high salinities. The IRGA was calibrated after returning to the ship, but while the analyzer was still cold. Data were stored on a Li-Cor Li-1400 data logger. All devices, except the peristaltic pump, were enclosed in an insulated box that contained a 12 V power source providing enough heat to keep the inside temperature just above 0 °C.

Ice cores were kept frozen during shipping for subsequent analysis of bulk ice pCO_2 at the Laboratoire de Glaciologie, Université Libre de Bruxelles, Belgium. The general principle of the method was to equilibrate the sea ice samples at the in situ temperature with a mixture of N_2 and CO_2 at known concentrations (so-called standard gas, in this study 396 µatm) and rapidly extract the gas into a Varian 3300 gas chromatograph under vacuum (Geilfus et al., 2012b). Each ice sample was cut into a 4 cm × 4 cm × 4.5 cm cube to tightly fit the equilibration container, thereby both minimizing the headspace and keeping it consistent. The standard gas was injected at 1013 mbar into the equilibration container containing the ice sample. Then the container was placed in a

thermostated bath at the in situ temperature. After 24 h, the ice sample was assumed to have returned to the brine volume and chemical conditions at the in situ temperature and to have equilibrated ($> 90\%$) with the standard gas, which was then injected into the gas chromatograph. The pressure difference between the vacuum line and the container forced all the remaining CO_2 (i.e. CO_2 not yet in equilibrium with the standard gas) to be rapidly extracted from the brine into the line of the gas chromatograph. This method is only valid if the ice is permeable at the in situ conditions (Geilfus et al., 2012b).

Air–ice CO_2 fluxes were measured using an accumulation chamber (West System) placed on top of the ice. The chamber was a metal cylinder closed at the top, with an internal diameter of 20 cm and an internal height of 9.7 cm. A rubber seal surrounded by a serrated steel edge ensured an airtight connection between the ice and the chamber. For the measurements over snow, a steel tube was mounted at the base of the chamber to enclose snow down to the ice and prevent lateral infiltration of air through the snow. The chamber was connected in a closed loop to the IRGA with an air pump rate of $3\,L\,min^{-1}$. The pCO_2 in the chamber was recorded every 30 s for at least 5 min. The flux was computed from the slope of the linear regression of pCO_2 vs. time ($r^2 > 0.99$) according to Frankignoulle (1988), taking into account the volume of ice or snow enclosed within the chamber. The uncertainty of the flux computation due to the standard error on the regression slope was, on average, $\pm 3\%$.

3 Results

3.1 Atmospheric conditions

During the 2007 winter–spring transition in the Bellingshausen Sea, several low-pressure systems of varying intensity and length occurred at the sampling location. Fluctuations in the air temperature are shown in Fig. 3, along with the surface ice temperature measured at each station. At least three successive cycles of warming and

cooling were recorded with temperatures ranging from 0.5 to −20 °C. These cycles consisted of warm atmospheric fronts from the north, generally accompanied by high velocity winds and precipitation, followed by cold air temperatures and little precipitation (Lewis et al., 2011; Vancoppenolle et al., 2011).

3.2 Sea ice and snow conditions

The Brussels and Liège sites had contrasting conditions in snow, ice thickness and ice texture (Fig. 2). Sea–ice conditions from both sites are fully described by Lewis et al. (2011), and profiles of temperature, bulk ice salinity, calculated brine salinity and brine volume, and δ^{18}O at the Brussels and Liège sites are given in Fig. 4.

At the Brussels site, the ice thickness, as determined by coring, ranged from 55 to 67 cm, while the snow cover ranged from 8 to 25 cm (Fig. 2a). The ice freeboard relative to seawater level, measured on each sampling event, was positive at all times and ranged from 0.7 to 3 cm. The ice cover was mainly composed of columnar crystals. The ice temperatures ranged from −1.5 to −6.1 °C. The main changes in temperatures were observed in the top 40 cm of the ice cover, oscillating between cooling and warming events within a 1 °C temperature window (from −3 to −4 °C), except on 16 October (Bxl 4), when the ice temperature decreased to −6.1 °C (Fig. 4). The bulk ice salinity ranged from 3.4 to 14.1. The profiles were typically S-shaped, as described by Eicken (1992), with higher salinities (from 11.5 to 14.1) in the top layer, dropping to minimum values (on average, $S = 4.1$) at the bottom. The evolution of the calculated brine salinity mirrored the evolution of the ice temperature, exhibiting an inverse relationship. From 1 to 16 October (Bxl 1 to Bxl 4), the brine salinities increased from the bottom to the top of the ice cover, with values close to seawater ($S = 34$) at the bottom to a maximum of 101 at the top on 16 October. On 16 October (Bxl 4), the top 20 cm of the ice cover had a brine volume lower than 5 %, which is considered as the percolation threshold above which columnar sea ice is considered permeable to fluid transport (Golden et al., 1998, 2007). The δ^{18}O isotopic ratio ranged from −5.8 to 2.1 ‰. On all sampling dates,

Title Page

Abstract | Introduction

Conclusions | References

Tables | Figures

|◄ | ►|

◄ | ►

Back | Close

Full Screen / Esc

Printer-friendly Version

Interactive Discussion

the top 20 cm showed negative $\delta^{18}O$ values while the rest of the profile showed $\delta^{18}O$ values around +1‰.

At the Liège site, the ice and snow cover were thicker than at the Brussels site and ranged from 99 to 106 cm and from 28 to 38 cm, respectively (Fig. 2b). The ice freeboard, initially positive (i.e. ice–snow interface above the seawater level) became negative on 18 and 23 October (Lg 4 and 5), and led to a flooding of the snow–ice interface. The ice cover at the Liège site was mainly composed of granular sea ice with inclusions of columnar and snow ice layers at different levels in the ice profile. These inclusions, associated with positive $\delta^{18}O$ (Fig. 4), suggest a formation under dynamic conditions with subsequent rafting events (Lewis et al., 2011). The observed variations of the bulk ice temperature and salinity, as well as the calculated brine salinity, were smaller than those observed at Brussels (Fig. 4). The ice temperature ranged from −1.3 to −3.7 °C. The ice cover showed similar warm and isothermal profiles on 3 and 8 October (Lg 1 and 2), with brine salinities similar to seawater values throughout the ice column. The ice cover cooled from 13 to 18 October (Lg 3 to 4), when the minimum temperature and maximum brine salinity were observed, as we also observed at the Brussels site. The calculated brine salinities mirrored the evolution of the ice temperature, increasing from 3 to 18 October (Lg 1 to 4), with values as high as 64. The bulk ice salinity ranged from 2.3 to 13.8, and the salinity profiles were also typically S-shaped, with the top layer ranging from 6.5 to 13.8, while the salinity of the bottom layer was, on average, 3. The calculated brine volume fraction was always above 5 %. The $\delta^{18}O$ isotopic ratio ranged from −4.9 to 2.9‰. At the top of the ice, $\delta^{18}O$ was negative from 3 to 13 October (Lg 1 to 3) and positive on our last two sampling days (Lg 4 and 5). In the lower half of the profiles, $\delta^{18}O$ values were generally around 1‰, although the cores sampled on 18 and 23 October (Lg 4 and 5) had negative $\delta^{18}O$ incursions, indicative of ice rafting, as suggested above.

Full Screen / Esc

3.3 Carbonate system

At the Brussels site, TA in sackhole brines ranged from 2406 to 4855 μmol kg^{-1} while TCO$_2$ ranged from 2288 to 4110 μmol kg^{-1} (Fig. 5). Changes in TA and TCO$_2$ closely mimicked the salinity changes. Normalizing TA and TCO$_2$ to a salinity of 34 (denoted as nTA and nTCO$_2$) showed how sensitive these parameters were to salinity changes. Indeed, both nTA and nTCO$_2$ remain relatively stable, around 2350 μmol kg^{-1} for nTA and 2010 μmol kg^{-1} for nTCO$_2$. The pH$_T$ ranged from 7.9 to 8.8 and increased continuously during the survey, except for a significant decrease in the deeper brine on 16 October (Bxl 4; Fig. 5). This decrease was associated with a decrease in the brine salinity and TA. The in situ brine pCO$_2$ ranged from 82 to 392 μatm. The brines were undersaturated in CO$_2$, relative to the atmosphere (383.8 μatm in 2007), except on 16 October (Bxl 4, Figs. 5 and 6). The brine pCO$_{2calc}$ was consistent within 50 μatm with the brine pCO$_2$ measured in situ, except on 1 October (Bxl 1) when brine pCO$_{2calc}$ was extremely high, at 620 μatm (Fig. 5). From 1 to 6 October (Bxl 1 to 2), the in situ brine pCO$_2$ values were from 210 to 271 μatm (Fig. 6). Then, the in situ brine pCO$_2$ decreased on 11 October (Bxl 3) and increased again on 16 October (Bxl 4) to concentrations ranging from 248 to 392 μatm. On 21 October (Bxl 5), the in situ brine pCO$_2$ decreased down to concentrations ranging from 82 to 115 μatm. The bulk ice pCO$_2$ ranged from 15 to 150 μatm (Fig. 6), generally increasing with depth and lower than the brine pCO$_2$.

At the Liège site, the brine salinity ranged from 38.1 to 58.3. TA ranged from 2806 to 4074 μmol kg^{-1} while TCO$_2$ ranged from 1826 to 3590 μmol kg^{-1} (Fig. 5). As for the Brussels site, TA and TCO$_2$ changes seem closely related to salinity changes, except on 3 October (Lg 1). Indeed, nTA and nTCO$_2$ decreased from 3560 and 3155 μmol kg^{-1}, respectively, to stabilize around 2356 and 1817 μmol kg^{-1}, respectively. The pH$_T$ ranged from 8.5 to 8.7 with a significant increase on 13 October (Lg 3) to a reported maximum of 9.2 (Fig. 5). The in situ brine pCO$_2$ was undersaturated compared to the atmosphere, with values ranging from 65 to 183 μatm. These values

Title Page

Abstract | Introduction

Conclusions | References

Tables | Figures

◄ | ►|

◄ | ►

Back | Close

Full Screen / Esc

Printer-friendly Version

Interactive Discussion

were consistent within 80 µatm with the brine pCO_{2calc}. Changes of the in situ brine pCO_2 were smaller than the variations at the Brussels site. The most significant change occurred on 18 October (Lg 4) where the in situ brine pCO_2 increased to concentrations ranging from 147 to 183 µatm. The bulk ice pCO_2 ranged from 9 to 193 µatm (Fig. 6). Bulk ice pCO_2 were here generally more consistent with brine pCO_2, except in the colder 8 and 18 October stations (Lg 2 and 4).The minimum concentrations were observed in the top 20 cm of the ice cover while the maximum concentrations were observed at the sea ice interface with the underlying seawater. The mean bulk ice pCO_2 ranged from 70 to 79 µatm from 3 to 18 October (Lg 1 to 4) and increased to 97 µatm on 23 October (Lg 5).

The salinity and CO_2 system parameters were relatively constant in the underlying seawater during our survey (Fig. 7). We observed a slight decrease in the salinity on 13 October (Lg 3), while pH_T decreased and TCO_2 increased on 11 and 13 October (Bxl 3 and Lg 3). The seawater pCO_2 measured in situ was supersaturated relative to the atmosphere, ranging from 401 to 462 µatm.

3.4 Air–ice CO_2 fluxes

The CO_2 fluxes measured at the sea ice and snow interfaces with the atmosphere suggest that, except for a small efflux of 0.3 mmol m^{-2} d^{-1} measured over the ice at the Brussels site on 16 October (Bxl 4), both the sea ice and the snow acted as sinks for atmospheric CO_2 during our study (Fig. 8). In general, Brussels sea ice showed a smaller uptake of atmospheric CO_2 that was not significantly different from zero (Fig. 8a). In Liège, the uptake of atmospheric CO_2 was more significant, ranging up to −2.9 mmol m^{-2} d^{-1} over sea ice, although the values were lower over snow (Fig. 8b).

4 Discussion

4.1 Snow cover and temperature control on carbon dynamics within sea ice

At the beginning of the sampling period, during early austral spring, the ice covers at stations Brussels and Liège were nearly isothermal and likely permeable throughout, as the brine volume was above 5 % (Fig. 4, Golden et al., 2007). Subsequently, the succession of warm and cold events with passing atmospheric fronts (Fig. 3) affected the temperature gradient within the ice cover significantly. At both sites, the fluctuations in ice temperature occurred mainly in the top 40 cm (Fig. 4). Lewis et al. (2011) suggested that snow thickness was a key component in regulating the heat fluxes and morphological changes in the sea ice during our study. The ice at the Brussels site had little snow accumulation (Fig. 2) and larger temperature changes than the Liège site (Fig. 4) where the snow cover was thicker and insulated the underlying sea ice cover. Indeed, snow has a low thermal conductivity, about an order of magnitude lower than that of sea ice, and therefore acts as a thermal insulator (Massom et al., 2001).

At the Brussels site, the high brine salinities at the top of the ice resulted in an unstable salinity gradient within the ice cover (Fig. 4). This may have initiated convection, with brines moving downward through the ice cover to be replaced by underlying seawater moving upward (Lewis et al., 2011). Brabant (2012) suggested that brine drainage could have occurred between 1 and 6 October and between 11 and 16 October at the Brussels site. At the Liège site, the larger accumulation of snow muted the thermal fluctuations within the sea ice and, therefore, the changes in brine volume and salinity. Hence, the variations in brine salinity and in the resulting density gradient were more moderate at Liège (Fig. 4).

The presence of a thick snow cover also provided overburden that resulted in negative freeboard (Fig. 2). The negative freeboard observed at the Liège site toward the end of our study, associated with a permeable sea ice cover with an interconnected brine network, allowed flooding of the ice surface and promoted the formation of a saline slush layer (Eicken et al., 1994; Lewis et al., 2011). Such flooding during

our study was also confirmed by Brabant (2012) using nutrient distributions within the ice cover. The flooding of the ice cover at the Liège site on 18 October could explain the observed increase in both TA and brine pCO_2 (Fig. 5), because pCO_2 was high in the surface seawater (Fig. 7). However, the increases in TA and pCO_2 in the ice could also be solely due to the decrease in the ice temperature (Fig. 4) and the associated increase in the brine salinities (Fig. 5). Indeed, the brine salinity seems to be the main control on the brine carbonate system, as both nTA and nTCO$_2$ from both stations were relatively constant through most of the sampling period. The small scatter in the nTCO$_2$ concentrations could simply be due to errors in calculating nTCO$_2$ from TA and pH$_T$. In addition, we assumed that the equilibrium constants we used in that calculation are valid at subzero temperatures and high salinities, and the general agreement between the measured and calculated brine pCO_2 values (Fig. 5) seems to validate this assumption. Only on 1 October (Bxl 1) did the measured and calculated brine pCO_2 values differ substantially, possibly because of errors in any of the measured parameters on that first day of sampling.

The generally higher brine salinities at the Brussels site, compared to Liège, (Figs. 4 and 5) were associated with higher TA, TCO$_2$, and in situ pCO_2 and lower pH$_T$ (Fig. 5). These differences were expected, because most solute concentrations increase with brine salinity, which also decreases CO_2 solubility (Papadimitriou et al., 2004). The Brussels site had little snow cover and larger temperature changes within the upper layer of the ice than the Liège site. Therefore, the differences in salinity, TA, pH$_T$, TCO$_2$ and pCO_2 between the upper and lower brines were generally greater at Brussels than at Liège (Fig. 5). However, convection events between 1 and 6 October appear to have homogenized both brine depths. The low atmospheric temperatures on 4–5 October (Fig. 3) cooled the ice surface (Fig. 4), increased the brine salinity and likely initiated convection (Brabant, 2012), thereby homogenizing salinity, TA, pH$_T$, TCO$_2$ and pCO_2 between the two-sackhole depths sampled on 6 October (Bxl 2). On 16 October, the decrease in the brine volume below the 5 % level (Fig. 4) made the upper layer less permeable and isolated it from those below. This promotes the large differences observed

in salinity, TA, TCO$_2$ and pH$_T$ between the upper layer and lower brine samples. At station Liège, where the thermal fluctuations in the ice cover were damped by the thicker snow cover, we saw only minor differences in salinity, TA, pH$_T$, TCO$_2$ and in situ pCO$_2$ between the upper and lower brine depths, and indeed Ra numbers in Brabant (2012)

5   indicate no significant convection events, which however does not rule out flooding, as mentioned earlier on.

     Brine pCO$_2$ and, to a lesser extent, bulk ice pCO$_2$ both seem to follow the variations in the ice temperatures with the succession of warm and cold events (Fig. 6). Each time the ice cover cooled the pCO$_2$ increased slightly (e.g., on 6 and 16 October at

10   the Brussels site and on 18 October at the Liège site; Figs. 4 and 5), and conversely, pCO$_2$ dropped as temperatures rose (e.g., on 11 and 21 October at Brussels and on 23 October at Liège). Because pCO$_2$ is highly dependent on temperature, the changes in both brine and bulk ice pCO$_2$ were larger at the Brussels site than at Liège having thicker insulating layer of snow. In addition, the greater changes in porosity throughout

15   the ice column at the Brussels site (Fig. 4) led to more variability in brine pCO$_2$ than in the bulk ice (Fig. 6). At the Liège site, the pCO$_2$ variations were more limited, due to the smaller variations in ice temperature under the thicker snow cover (Fig. 4). However, the flooding observed on 18 and 23 October (Lg 4 and 5) could explain the increase of the in situ brine and bulk ice pCO$_2$ due to the input of high pCO$_2$ seawater (Fig. 6).

20   From Fig. 6, the in situ brine pCO$_2$ values are more variable than those in bulk ice. Sampling brines using the sackhole technique provides the advantage of a direct in situ measurement, but the origin of the brine that collects in the sackhole is unknown, and only brine that can move easily within the ice matrix is sampled. In addition, sackhole brines are subject to air–sea exchange during sampling, and, at the low pCO$_2$ values

25   we observed during our study, the brines could very well have absorbed at least some CO$_2$ from the atmosphere before we completed our measurements. In comparison, our bulk ice pCO$_2$ analyses address brine located in a well-defined location within the sea ice and include both brines and gas bubbles trapped within the ice matrix. It should be stressed that small brine pockets trapped and isolated in the ice matrix will not be

sampled using the sackhole technique but will, on the contrary, be included in the bulk ice pCO$_2$ measurement. Indeed, brines collected using the sackhole technique represent the most mobile part of brines, those located in relatively large and connected brine channels. Thus, the sackhole brines are most susceptible to exchange CO$_2$ with the atmosphere and mixing with the underlying, high pCO$_2$, seawater due to flooding or participation in convection events. Therefore, the bulk ice pCO$_2$ values changes are less variable, reflecting mostly internal melting due to temperature and salinity changes in the ice cover while sackhole brines highlight rapid changes in the brine network due, for example, to a cooling/warming event in the ice, input of high pCO$_2$ seawater or from brine convection and possible contamination from the contact with the atmosphere during the 10–60 min time window.

4.2 Biological controls on carbon dynamics within sea ice

Dumont (2009) presented a complete description of the distributions and concentrations of organic matter, including chlorophyll *a* (Fig. 9) in the ice at both the Brussels and Liège sites. The vertical Chl *a* distributions were more variable at the Liège site than at Brussels, but at neither site were the variations in Chl *a* associated with the changes in pCO$_2$. The one exception was during the flooding event at Liège 18 to 23 October, which apparently increased Chl *a*, as well as pCO$_2$.

4.3 Antarctic sea ice as a spring-time sink of atmospheric CO$_2$ – comparison with the Arctic.

The bulk ice pCO$_2$ values observed during the present study in Antarctic are within the same range as those few records existing in the Arctic; Barrow, Alaska (Geilfus et al., 2012b), and Resolute Bay, Canada (Geilfus et al., 2014) (Fig. 10), where sampling also included melting, nearly isothermal first-year landfast sea ice in late spring (June). Higher pCO$_2$ values were reported (Geilfus et al., 2012b; Crabeck et al., 2014) in sea ice from early spring at Barrow and from SW Greenland, respectively. Although based

on a limited data-set, existing data suggests that Antarctic sea ice may generally have lower pCO_2 values than Arctic sea ice at the same temperature (Fig. 10), as suggested by Geilfus et al. (2012a). Even if the data are still too sparse to confidently affirm that Antarctic sea ice is lower in pCO_2, it is noteworthy that the range of concentrations observed in this study suggests that Antarctic sea ice becomes undersaturated in CO_2, relative to the atmosphere, early in the winter–spring transition, reaching levels not observed in Arctic sea ice until much later in the spring decay process (Geilfus et al., 2012a, b; 2014; Crabeck et al., 2014). From the Fig. 10c, we can observe that at low brine volume, sea ice has a high bulk ice pCO_2. The brine volume combines the effect of the high salinity and low temperature at the same time. It should also be noted that both in the Arctic and in the Antarctic, spring sea ice can become undersaturated in CO_2, while the underlying seawater is still supersaturated (Fig. 7) (Papakyriakou and Miller, 2011).

During this study, we observed a net uptake of atmospheric CO_2 by the snow and sea ice at both sites. This uptake was of the same order of magnitude as previous fluxes reported over Antarctic sea ice during the austral summer by Delille (2006) and Nomura et al. (2013) and over Arctic sea ice by Semiletov et al. (2004), Nomura et al. (2010a, b), and Geilfus et al. (2012a, 2013, 2014), using similar chamber techniques. At the Brussels site, fluxes measured over snow were similar to those measured over bare ice (after removing the snow cover, Fig. 8). This suggests that the thin snow cover had a limited impact on the CO_2 exchange. At the Liège site, the thicker snow cover seemed to reduce the magnitude of the fluxes. The snow cover could have acted as a buffer between the ice and the atmosphere, as suggested by Miller et al. (2011). However, in contrast to Nomura et al. (2010b), a snow cover thicker than 9 cm did not seem to completely prevent the CO_2 exchanges between the ice and the atmosphere at our study sites. As suggested by Delille (2006), Nomura et al. (2010a, 2013), and Geilfus et al. (2012a), the magnitude of the CO_2 fluxes depends on the pCO_2 gradient between the ice and the overlying atmosphere.

5 Conclusions

A succession of warming and cold events during the SIMBA expedition had a strong impact on the sea–ice cover, both its physical properties (Lewis et al., 2011) and inorganic carbon dynamics. In particular, the snow thickness was likely the key component regulating the heat flux and thereby the temperature and salinity regime within the sea ice (Lewis et al., 2011). Our observations suggest that the snow is a key component in the changes occurring in the carbonate system within the sea ice.

The sampling site with less snow accumulation and larger temperature variations also had larger variations in brine salinity, TA, TCO_2, and brine and bulk ice pCO_2. In addition, the combination of unstable salinity gradients within the ice cover and episodic warming events initiated brine convection at the low-snow site on two occasions, which homogenized brine characteristics throughout the ice column. At the end of the survey, some flooding events took place at the high-snow site, bringing high pCO_2 seawater into the ice cover.

Our results highlight differences in the dynamics of pCO_2 as measured in bulk ice vs. sackhole brines. The bulk ice pCO_2 values were much less variable, reflecting mostly internal, temperature and salinity driven thermodynamic changes, while pCO_2 variations in sackhole brines reflected rapid transport within the brine channel network, as well as exchange with the atmosphere and underlying surface waters.

At both sampling sites, the ice cover acted as a sink for atmospheric CO_2, even despite episodic flooding by supersaturated seawater. Thus, during this early spring period the carbonate system in the sea ice of the Bellingshausen Sea behaved as a transition layer between the ocean and the atmosphere, reacting to atmospheric forcing, and largely independent of the seawater conditions.

References

Brabant, F.: Physical and Biogeochemical Controls on the DMS/P/O Cycle in Antarctic Sea Ice, Universite Libre de Bruxelles, Bruxelles, 300 pp., 2012.

Copin Montégut, C.: A new formula for the effect of temperature on the partial pressure of carbon dioxide in seawater, Mar. Chem., 25, 29–37, 1988.

Cox, G. F. N. and Weeks, W. F.: Equations for determining the gas and brine volumes in sea–ice samples, J. Glaciol., 29, 306–316, 1983.

Crabeck, O., Delille, B., Thomas, D. N., Geilfus, N. X., Rysgaard, S., and Tison, J. L.: CO_2 and CH_4 in sea ice from a subarctic fjord, Biogeosciences Discuss., 11, 4047–4083, doi:10.5194/bgd-11-4047-2014, 2014.

Delille, B.: Inorganic Carbon Dynamics and Air–Ice–Sea CO_2 Fluxes in the Open and Coastal Waters of the Southern Ocean, Université de Liège, Liège, 296 pp., 2006.

Delille, B., Jourdain, B., Borges, A. V., Tison, J. L., and Delille, D.: Biogas (CO_2, O-2, dimethyl-sulfide) dynamics in spring Antarctic fast ice, Limnol. Oceanogr., 52, 1367–1379, 2007.

Delille, B., Vancoppenolle, M., Geilfus, N. X., Tilbrook, B., Lannuzel, D., Schoemann, V., Bec-quevort, S., Carnat, G., Borges, A. V., Delille, D., lancelot, C., Chou, L., Dieckmann, G. S., and Tison, J.-L.:. Southern Ocean sink: the contribution of the marine cryosphere, J. Geo-phys. Res.-Oceans, accepted, 2014.

Dickson, A. G. and Millero, F. J.: A comparison of the equilibrium constants for the dissociation of carbonic acid in seawater media, Deep-Sea Res., 34, 1733–1743, 1987.

Dieckmann, G. S. and Hellmer, H. H.: The importance of sea ice: an overview, in: Sea Ice, edited by: Thomas, D. N. and Dieckmann, G. S., 2nd Edn., Wiley-Blackwell, Oxford, 1–22, 2010.

DOE: Handbook of methods for the analysis of the various parameters of the carbon dioxide system in sea water, version 2, edited by: Dickson, A. G. and Goyet, C., ORNL/CDIAC-74, 1994.

Dumont, I.: Interactions Between the Microbial Network and the Organic Matter in the Southern Ocean: Impacts on the Biological Carbon Pump, Université Libre de Bruxelles, Bruxelles, 202 pp., 2009.

Eicken, H.: Salinity profiles of Antarctic sea ice – field data and model results, J. Geophys. Res.-Oceans, 97, 15545–15557, 1992.

Eicken, Hajo, Lange, Manfred A., and Wadhams, Peter: Characteristics and distribution patterns of snow and meteoric ice in the Weddell Sea and their contribution to the mass balance of sea ice, Ann. Geophys., 12, 80–93, doi:10.1007/s00585-994-0080-x, 1994.

Frankignoulle, M.: Field-measurements of air sea CO_2 exchange, Limnol. Oceanogr., 33, 313–322, 1988.

Frankignoulle, M. and Borges, A. V.: Direct and indirect pCO_2 measurements in a wide range of pCO_2 and salinity values (the Scheldt estuary), Aquat. Geochem., 7, 267–273, 2001.

Geilfus, N.-X., Carnat, G., Papakyriakou, T., Tison, J.-L., Else, B., Thomas, H., Shadwick, E., and Delille, B.: Dynamics of pCO_2 and related air-ice CO_2 fluxes in the Arctic coastal zone (Amundsen Gulf, Beaufort Sea), J. Geophys. Res., 117, C00G10, doi:10.1029/2011JC007118, 2012a.

Geilfus, N. X., Delille, B., Verbeke, V., and Tison, J. L.: Towards a method for high vertical resolution measurements of the partial pressure of CO_2 within bulk sea ice, J. Glaciol., 58, 287–300, 2012b.

Geilfus, N. X., Carnat, G., Dieckmann, G. S., Halden, N., Nehrke, G., Papakyriakou, T., Tison, J. L., and Delille, B.: First estimates of the contribution of $CaCO_3$ precipitation to the release of CO_2 to the atmosphere during young sea ice growth, J. Geophys. Res., 118, 224–255, doi:10.1029/2012JC007980, 2013.

Geilfus, N.-X., Galley, R. J., Crabeck, O., Papakyriakou, T., Landy, J., Tison, J.-L., and Rysgaard, S.: Inorganic carbon dynamics of melt pond-covered first year sea ice in the Canadian Arctic, Biogeosciences Discuss., 11, 7485–7519, doi:10.5194/bgd-11-7485-2014, 2014.

Impact of snow cover on CO_2 dynamics in Antarctic pack ice

N.-X. Geilfus et al.

Title Page

Abstract	Introduction
Conclusions	References
Tables	Figures

|◄ | ►|

◄ | ►

Back | Close

Full Screen / Esc

Printer-friendly Version

Interactive Discussion

Gleitz, M., v.d. Loeff, M. R., Thomas, D. N., Dieckmann, G. S., and Millero, F. J.: Comparison of summer and winter inorganic carbon, oxygen and nutrient concentrations in Antarctic sea ice brine, Mar. Chem., 51, 81–91, 1995.

Golden, K. M., Ackley, S. F., and Lytle, V. I.: The percolation phase transition in sea ice, Science, 282, 2238–2241, 1998.

Golden, K. M., Eicken, H., Heaton, A. L., Miner, J., Pringle, D. J., and Zhu, J.: Thermal evolution of permeability and microstructure in sea ice, Geophys. Res. Lett., 34, L16501, doi:10.1029/2007GL030447, 2007.

Gran, G.: Determination of the equivalence point in potentiometric titration, Part II, Analyst, 77, 661–671, 1952.

Leppäranta, M. and Manninen, T.: The brine and gas content of sea ice with attention to low salinities and high temperatures, Rep., Finnish Institute of Marine Research, Helsinki, 15 pp., 1988.

Lewis, M. J., Tison, J. L., Weissling, B., Delille, B., Ackley, S. F., Brabant, F., and Xie, H.: Sea ice and snow cover characteristics during the winter-spring transition in the Bellingshausen Sea: an overview of SIMBA 2007, Deep-Sea Res. Pt. II, 58, 1019–1038, 2011.

Marion, G. M.: Carbonate mineral solubility at low temperatures in the Na-K-Mg-Ca-H-Cl-SO$_4$-OH-HCO$_3$-CO$_3$-CO$_2$-H$_2$O system, Geochim. Cosmochim. Ac., 65, 1883–1896, 2001.

Massom, R. A., Eicken, H., Haas, C., Jeffries, M. O., Drinkwater, M. R., Sturm, M., Worby, A. P., Wu, X., Lytle, V. I., Ushio, S., Morris, K., Reid, P. A., Warren, S. G., and Allison, I.: Snow on Antarctic Sea ice, Rev. Geophys., 39, 413–445, 2001.

Mehrbach, C., Culberson, C. H., Hawley, J. E., and Pytkowicz, R. M.: Measurements of the apparent dissociation constants of carbonic acid in seawater at atmospheric pressure, Limnol. Oceanogr., 18, 897–907, 1973.

Miller, L. A., Chierici, M., Johannessen, T., Noji, T. T., Rey, F., and Skjelvan, I.: Seasonal dissolved inorganic carbon variations in the Greenland Sea and implications for atmospheric CO$_2$ exchange, Deep-Sea Res. Pt. II, 46, 1473–1496, 1999.

Miller, L. A., Papakyriakou, T., Collins, R. E., Deming, J., Ehn, J., Macdonald, R. W., Mucci, A., Owens, O., Raudsepp, M., and Sutherland, N.: Carbon dynamics in sea ice: a winter flux time series, J. Geophys. Res.-Oceans, 116, C02028, doi:10.1029/2009JC006058, 2011.

Nomura, D., Eicken, H., Gradinger, R., and Shirasawa, K.: Rapid physically driven inversion of the air–sea ice CO$_2$ flux in the seasonal landfast ice off Barrow, Alaska after onset surface melt, Cont. Shelf Res., 30, 1998–2004, 2010a.

Title Page

Abstract | Introduction

Conclusions | References

Tables | Figures

◄ | ►

◄ | ►

Back | Close

Full Screen / Esc

Printer-friendly Version

Interactive Discussion

Nomura, D., Yoshikawa-Inoue, H., Toyota, T., and Shirasawa, K.: Effects of snow, snow-melting and re-freezing processes on air–sea ice CO_2 flux, J. Glaciol., 56, 262–270, 2010b.

Nomura, D., Granskog, M. A., Assmy, P., Simizu, D., and Hashida, G.: Arctic and Antarctic sea ice acts as a sink for atmospheric CO_2 during periods of snowmelt and surface flooding, J. Geophys. Res.-Oceans, 118, 6511–6524, doi:10.1002/2013JC009048, 2013.

Papadimitriou, S., Kennedy, H., Kattner, G., Dieckmann, G. S., and Thomas, D. N.: Experimental evidence for carbonate precipitation and CO_2 degassing during sea ice formation, Geochim. Cosmochim. Ac., 68, 1749–1761, 2004.

Papadimitriou, S., Thomas, D. N., Kennedy, H., Haas, C., Kuosa, H., Krell, A., and Dieckmann, G. S.: Biogeochemical composition of natural sea ice brines from the Weddell Sea during early austral summer, Limnol. Oceanogr., 52, 1809–1823, 2007.

Papakyriakou, T. and Miller, L.: Springtime CO_2 exchange over seasonal sea ice in the Canadian Arctic Archipelago, Ann. Glaciol., 52, 215–224, doi:10.3189/172756411795931534 , 2011.

Parmentier, F.-J. W., Christensen, T. R., Sørensen, L. L., Rysgaard, S., McGuire, A. D., Miller, P. A., and Walker, D. A.: The impact of lower sea–ice extent on Arctic greenhouse-gas exchange, Nature Climate Change, 3, 195–202, doi:10.1038/nclimate1784 , 2013.

Rysgaard, S., Glud, R. N., Sejr, M. K., Bendtsen, J., and Christensen, P. B.: Inorganic carbon transport during sea ice growth and decay: a carbon pump in polar seas, J. Geophys. Res.-Oceans, 112, C03016, doi:10.1029/2006JC003572, 2007.

Rysgaard, S., Bendtsen, J., Delille, B., Dieckmann, G. S., Glud, R. N., Kennedy, H., Mortensen, J., Papadimitriou, S., Thomas, D. N., and Tison, J. L.: Sea ice contribution to the air–sea CO(2) exchange in the Arctic and Southern Oceans, Tellus B, 63, 823–830, 2011.

Rysgaard, S., Glud, R. N., Lennert, K., Cooper, M., Halden, N., Leakey, R. J. G., Hawthorne, F. C., and Barber, D.: Ikaite crystals in melting sea ice – implications for pCO_2 and pH levels in Arctic surface waters, The Cryosphere, 6, 901–908, doi:10.5194/tc-6-901-2012, 2012.

Rysgaard, S., Søgaard, D. H., Cooper, M., Pućko, M., Lennert, K., Papakyriakou, T. N., Wang, F., Geilfus, N. X., Glud, R. N., Ehn, J., McGinnis, D. F., Attard, K., Sievers, J., Deming, J. W., and Barber, D.: Ikaite crystal distribution in winter sea ice and implications for CO_2 system dynamics, The Cryosphere, 7, 707–718, doi:10.5194/tc-7-707-2013, 2013.

Semiletov, I. P., Makshtas, A., Akasofu, S. I., and Andreas, E. L.: Atmospheric CO_2 balance: the role of Arctic sea ice, Geophys. Res. Lett., 31, L05121, doi:10.1029/2003GL017996, 2004.

Thomas, D. N. and Dieckmann, G. S.: Sea ice – an introduction to its physics, biology, chemistry and geology, in: Sea Ice, edited by: Thomas, D. N. and Dieckmann, G. S, 2nd Edn., Science, Oxford, UK, Wiley, Blackwell, p. 621, 2010.

Tison, J. L., Worby, A., Delille, B., Brabant, F., Papadimitriou, S., Thomas, D., de Jong, J., Lannuzel, D., and Haas, C.: Temporal evolution of decaying summer first-year sea ice in the Western Weddell Sea, Antarctica, Deep-Sea Res. Pt. II, 55, 975–987, 2008.

Vancoppenolle, M., Timmermann, R., Ackley, S. F., Fichefet, T., Goosse, H., Leonard, K. C., Lieser, J., Nicolaus, M., Papakyriakou, T., and Tison, J.-L.: Assessment of radiation forcing data sets for large-scale sea ice models in the Southern Ocean, Deep-Sea Res. Pt. II, 58, 1237–1249, 2011.

Weeks, W. F. (Ed.): On Sea Ice, Fairbanks, University of Alaska Press, Alaska, 664 pp., 2010.

Zemmelink, H. J., Delille, B., Tison, J. L., Hintsa, E. J., Houghton, L., and Dacey, J. W. H.: CO_2 deposition over the multi-year ice of the western Weddell Sea, Geophys. Res. Lett., 33, L13606, doi:10.1029/2006GL026320, 2006.

Title Page

Abstract | Introduction

Conclusions | References

Tables | Figures

◀ | ▶

◀ | ▶

Back | Close

Full Screen / Esc

Printer-friendly Version

Interactive Discussion
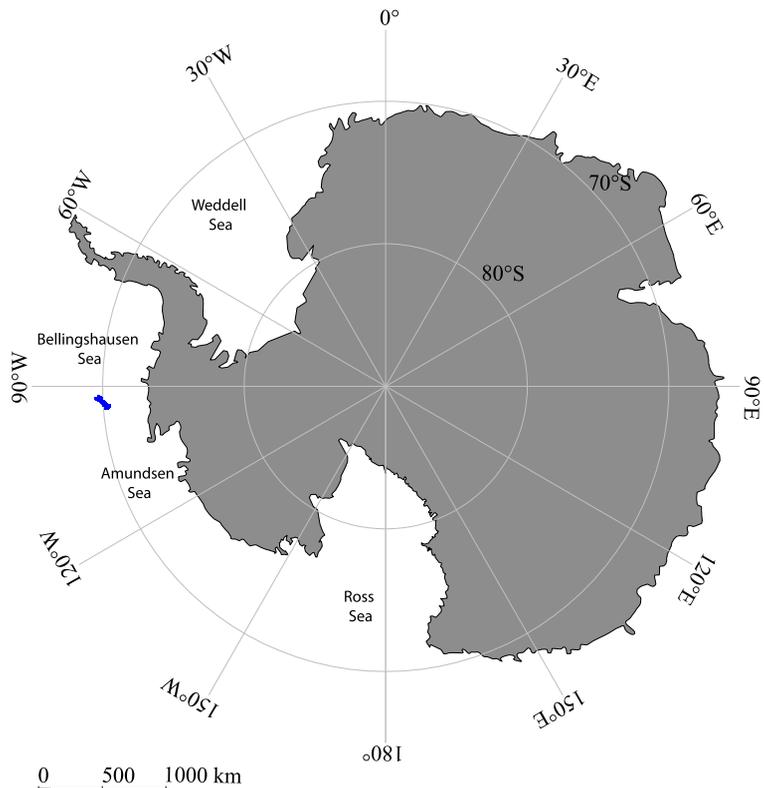
Figure 1. Location of the sampling area for the SIMBA cruise 2007, in the Bellingshausen Sea, Antarctica.

Title Page

Abstract | Introduction

Conclusions | References

Tables | Figures

Back | Close

Full Screen / Esc

Printer-friendly Version

Interactive Discussion

Figure 2. Ice (including range of observed values), snow thickness and freeboard at the Brussels and Liège sites.
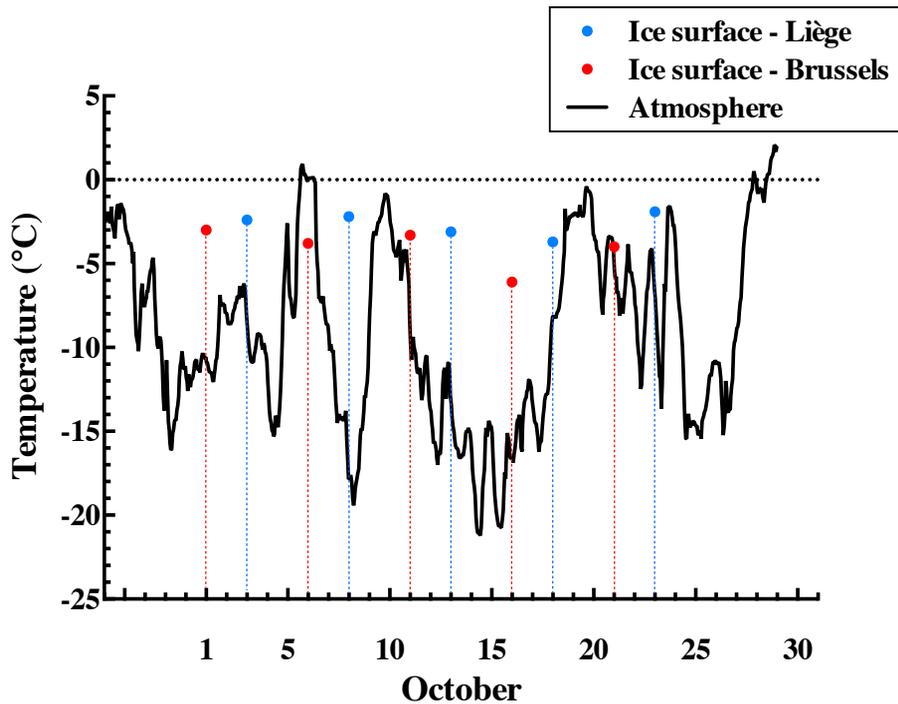
Figure 3. Daily time series of air temperature (˚C) recorded on the ship and the surface ice temperature of the different sampling stations at Brussels (red dots) and Liège (blue dots) site.

Figure 4. Profiles of temperature (˚C), bulk ice salinity, calculated brine salinity, brine volume fraction, and ^{18}O isotopic ratio from the Brussels (top) and Liège (bottom) sites.
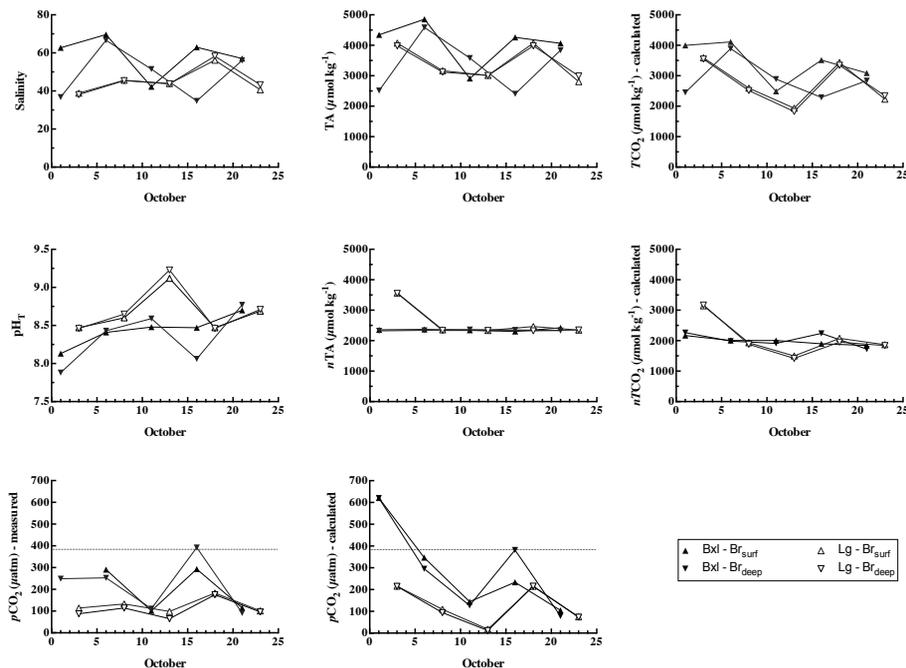
Figure 5. Evolution of salinity, pH_T, TA (in µmol kg^{-1}), nTA (TA normalized to a salinity of 34, in µmol kg^{-1}), calculated TCO$_2$ (in µmol kg^{-1}) and nTCO$_2$ (TCO$_2$ normalized to a salinity of 34, in µmol kg^{-1}), measured and calculated pCO$_2$ (in µatm) in surface and deep brine sackholes from the Brussels and Liège sites. The dotted line represents the atmospheric pCO$_2$ in October 2007.
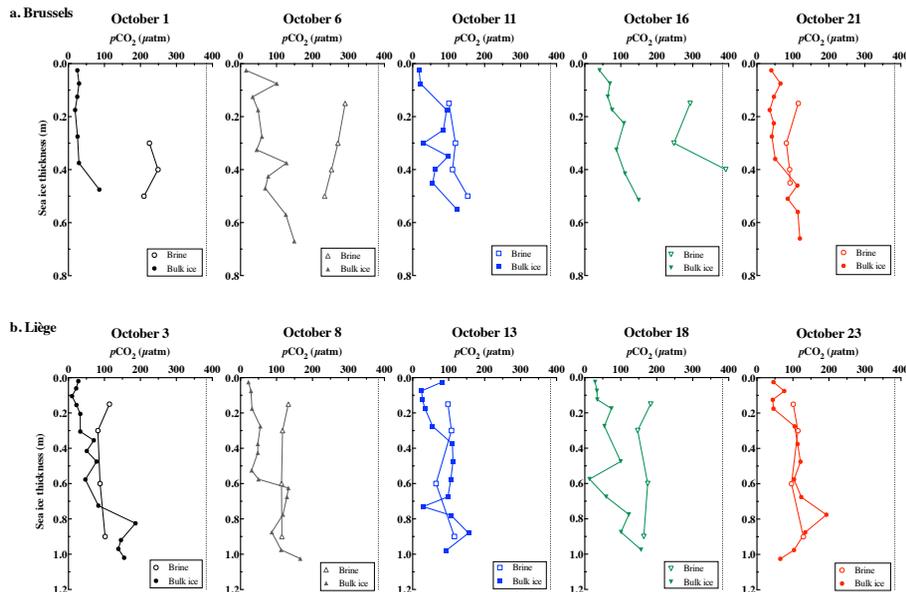
Figure 6. Vertical profiles of the in situ brine pCO_2 (in µatm) and bulk ice pCO_2 (in µatm) from the Brussels (top) and Liège (bottom) sites.
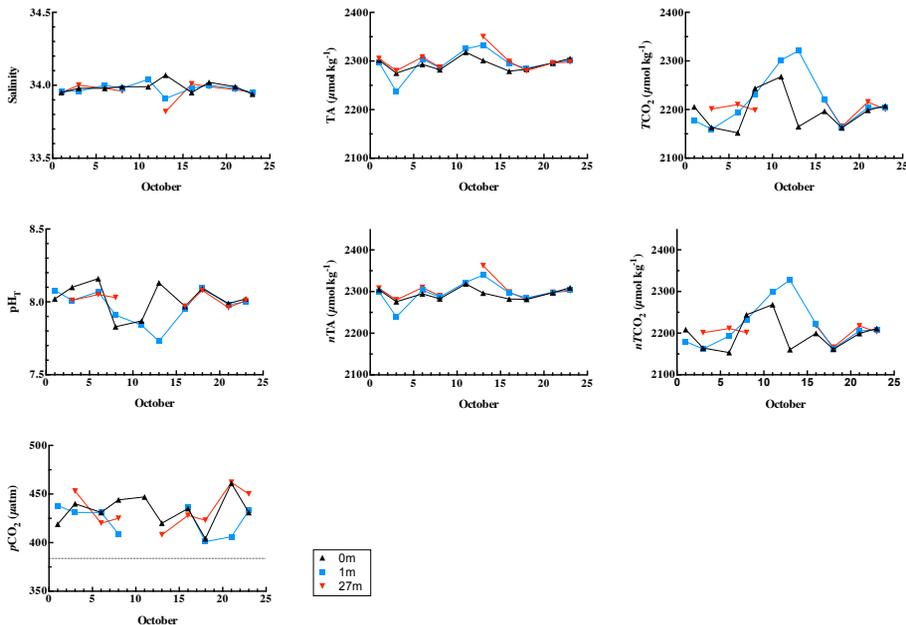
Figure 7. Evolution of salinity, pH$_T$, TA (in µmol kg^{-1}), nTA (TA normalized to a salinity of 34, in µmol kg^{-1}), calculated TCO$_2$ (in µmol kg^{-1}) and nTCO$_2$ (TCO$_2$ normalized to a salinity of 34, in µmol kg^{-1}), in situ pCO$_2$ (in µatm) in the underlying seawater at the ice–water interface and 1 and 27 m below the ice–water interface. The dotted line represents the atmospheric pCO$_2$ in 2007.

Figure 8. CO$_2$ fluxes (in mmol m^{-2} d^{-1}) measured over sea ice and snow for the Brussels and Liège sites.

Figure 9. Profiles of Chl *a* concentration within bulk sea ice at the Brussels and Liège sites, adapted from Dumont (2009).

Discussion Paper | Discussion Paper | Discussion Paper | Discussion Paper |

TCD

8, 3263–3295, 2014

Impact of snow cover on CO₂ dynamics in Antarctic pack ice

N.-X. Geilfus et al.

Title Page

Abstract | Introduction

Conclusions | References

Tables | Figures

|◄ | ►|

◄ | ►

Back | Close

Full Screen / Esc

Printer-friendly Version

Interactive Discussion
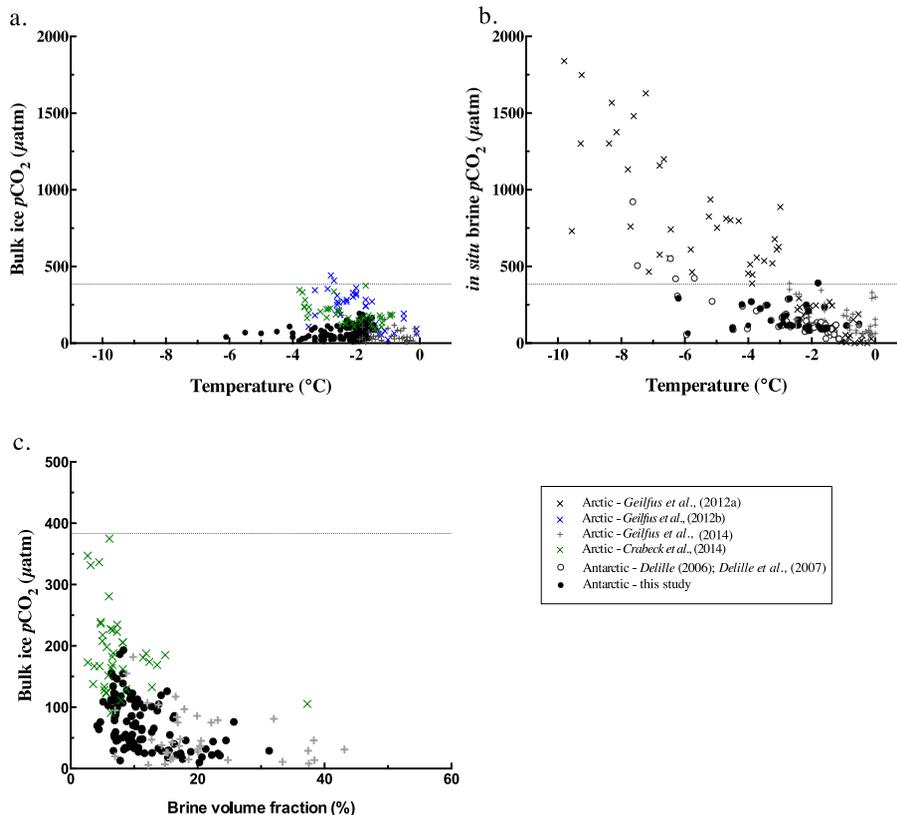
Figure 10. (a) The relationships between bulk ice pCO_2 (in µatm) and temperature measured in Antarctic (this study) and Arctic (Geilfus et al., 2012b, 2014; Crabeck et al., 2014) sea ice. **(b)** The relationships between in situ brine pCO_2 (in µatm) and brine temperature in Antarctic (this study; Delille, 2006; Delille et al., 2007) and Arctic sea ice (Geilfus et al., 2012a). **(c)** Relationship between the bulk ice pCO_2 (in µatm) and the brine volume fraction (in %) measured in Antarctic (this study) and Arctic (Geilfus et al., 2012b, 2014; Crabeck et al., 2014) sea ice.

Title Page

Abstract | Introduction

Conclusions | References

Tables | Figures

|◄ | ►|

◄ | ►

Back | Close

Full Screen / Esc

Printer-friendly Version

Interactive Discussion